

Short Communication

***In situ* Fabrication of Copper Nanocubes with Platinum Skin on 3D Graphene-Carbon Nanotubes Hybrid for Efficient Methanol Electrooxidation**

Genping Yi, Ziwen Chang, Guangzhen Liu, Liming Yang*

Key Laboratory of Jiangxi Province for Persistent Pollutants Control and Resources Recycle, Nanchang Hangkong University, Nanchang 330063, P. R. China

*E-mail: yangliming0809185@126.com (L. M. Yang)

Received: 7 November 2017 / Accepted: 19 March 2019 / Published: 30 June 2017

Tuning the macro-morphology and micro-structure simultaneously of platinum (Pt)-based electrocatalysts is pivotal for enhancing catalytic performance, but still remains great challenge. Herein, we first report elaborate copper nanocubes with Pt skin on 3D reduced graphene oxide-carbon nanotubes (rGO@CNTs) support. Graphene oxide is used as a surfactant to disperse pristine CNTs with a little CuSO₄ for electrochemical preparation of macro-morphological rGO@CNTs supporting Cu nanocubes, and subsequently reacted with H₂PtCl₆ solution *via* galvanic replacement to realize Pt skin micro-structure. Cyclic voltammetry and chronoamperometry technique indicate that the resultant Pt-Cu/rGO@CNTs catalyst is equipped with outstanding electrocatalytic activity and stability towards methanol oxidation reaction.

Keywords: Graphene; Carbon nanotubes; Cu nanocubes; Pt skin; Electrodeposition; Energy storage and conversion

1. INTRODUCTION

With the rapid growth of industrialization, a large amount of pollutants are being released into the aquatic environment, which has caused serious environmental challenges on a global scale [1–3]. Traditionally, platinum (Pt) is used as an anode catalyst towards methanol oxidation reaction (MOR) of direct methanol fuel cells (DMFCs) due to its high catalytic activity. However, high cost, easy poisoning and insufficient durability restrict the widespread use of Pt electrocatalysts. Various methods have been utilized to obtain highly efficient Pt-based catalysts, mainly including the control of micro-structure and the assembly of macro-morphology. The addition of other transition metal to develop Pt-based bi/multi-metallic catalysts is found to be effective through a bifunctional mechanism and/or an

electronic effect [4–6]. Maneuvering the shape could further promote their catalytic performances by micro-structure regulation [7, 8], however, frequently used bulky capping agents would cover the active sites and reduce the electric conductivity [9]. Facile and “clean” preparation of Pt-based nanocrystals with outer Pt-rich layers is a feasible way to obtain high-performance catalysts.

On the other hand, an effective support is necessary to realize the assembly of macro-morphology, and reduced graphene oxide (rGO)-CNTs hybrid is promising [10]. By acting as spacers for each other, graphene stacking and CNTs bundling are alleviated simultaneously to form a 3D architecture with high surface area, superior electrical conductivity and excellent chemical stability [11, 12]. However, pristine CNTs are generally needed chemical oxidative treatment and/or the use of polymeric surfactants, which could partially lower the conductivity and block the catalytic sites [13]. Therefore, *in situ* and “green” assembly of 3D interconnected rGO@CNTs macro-morphology supporting fine-tuning metal nanoparticles is desirable.

Herein, we report a Cu nanocubes with Pt skin anchored on 3D rGO@CNTs supporter by simple electrodeposition and galvanic replacement method. To our knowledge, this work represents the first example of *in situ* fabricating a 3D architecture of 1D CNTs and 2D rGO sheets supporting Cu nanocubes with Pt active layers. The resulting hybrid behaves as an excellent electrocatalyst for the MOR, with both high mass activity and better stability than a commercial Pt/C catalyst.

2. EXPERIMENTAL

2.1 Preparation of Pt-Cu/rGO@CNTs

Graphite oxide was prepared by the improved method with a minor modification. The as-prepared graphite oxide and the purchased CNTs were exfoliated in 0.1 M LiClO₄ solution by ultrasonication for 3 h to form 0.3 g L⁻¹ GO containing 0.3 g L⁻¹ CNTs black dispersion (denoted as GO-CNTs). Similarly, GO brown yellow dispersion was also prepared.

The Cu/rGO@CNTs hybrid was obtained by one-step electrodeposition of the GO-CNTs suspension and additional 0.8 mM CuSO₄ at a given potential of -1.2 V for 200 s on a CHI 660C electrochemical workstation with a three-electrode system: a glassy carbon electrode (GCE, 3 mm in diameter) as the working electrode, a Pt foil as the counter electrode, and a saturated calomel electrode (SCE) as the reference electrode. Cu/rGO hybrid was also prepared similarly without the addition of CNTs. The Cu/rGO@CNTs and Cu/rGO were immersed into 1.0 mM H₂PtCl₆ solution for 30 s. The Cu was partially replaced by Pt⁴⁺ during the process, and they are denoted as Pt-Cu/rGO@CNTs and Pt-Cu/rGO, respectively. The commercial Pt/C catalyst electrode was prepared by ultrasonically dispersing commercial Pt/C powder in ethanol solution containing Nafion (ν : ν = 20: 1) to form a 2.0 g L⁻¹ ink, and then casting the 10 μ L ink on a newly polished GC electrode.

The macro-morphology and micro-structure of the as-prepared materials were characterized by scanning electron microscope (SEM, Hitachi S-4800), transmission electron microscopy (TEM, JEM-3010) and high angle annular dark field-scanning TEM (HAADF-STEM, FEI Tecnai G² F20 S-TWIN).

2.2 Electrochemical measurements

The electrochemically active surface area (ECSA) values of the catalysts were determined by cyclic voltammetry (CV) method in N₂-saturated 0.5 M H₂SO₄ solution from -0.2 V to 1.2 V. The electrocatalytic activity for the MOR was characterized by CV measurement between 0 V and 1.0 V at a scan rate of 50 mV s⁻¹. The catalytic durability was performed by chronopotentiometry, and the given potential was 0.65 V for 800 s. The electrolyte is N₂-saturated 0.5 M H₂SO₄ solution containing 0.5 M CH₃OH.

3. RESULTS AND DISCUSSION

Compared to the flat-lying rGO nanosheets supported nanoparticles (Fig. S1), the introduction of CNTs make the structure more open to form 3D architecture which is in favor of rapid mass diffusion and fast electron transfer (Fig. 1a). The as-obtained Cu nanocubes are uniformly distributed on the 3D nanostructure. After partial replacement of Cu with Pt atoms, the Pt-Cu nanocrystal almost remains the nanocube micro-structure (Fig. 1b) and the 3D structure of the rGO@CNTs support is also reserved.

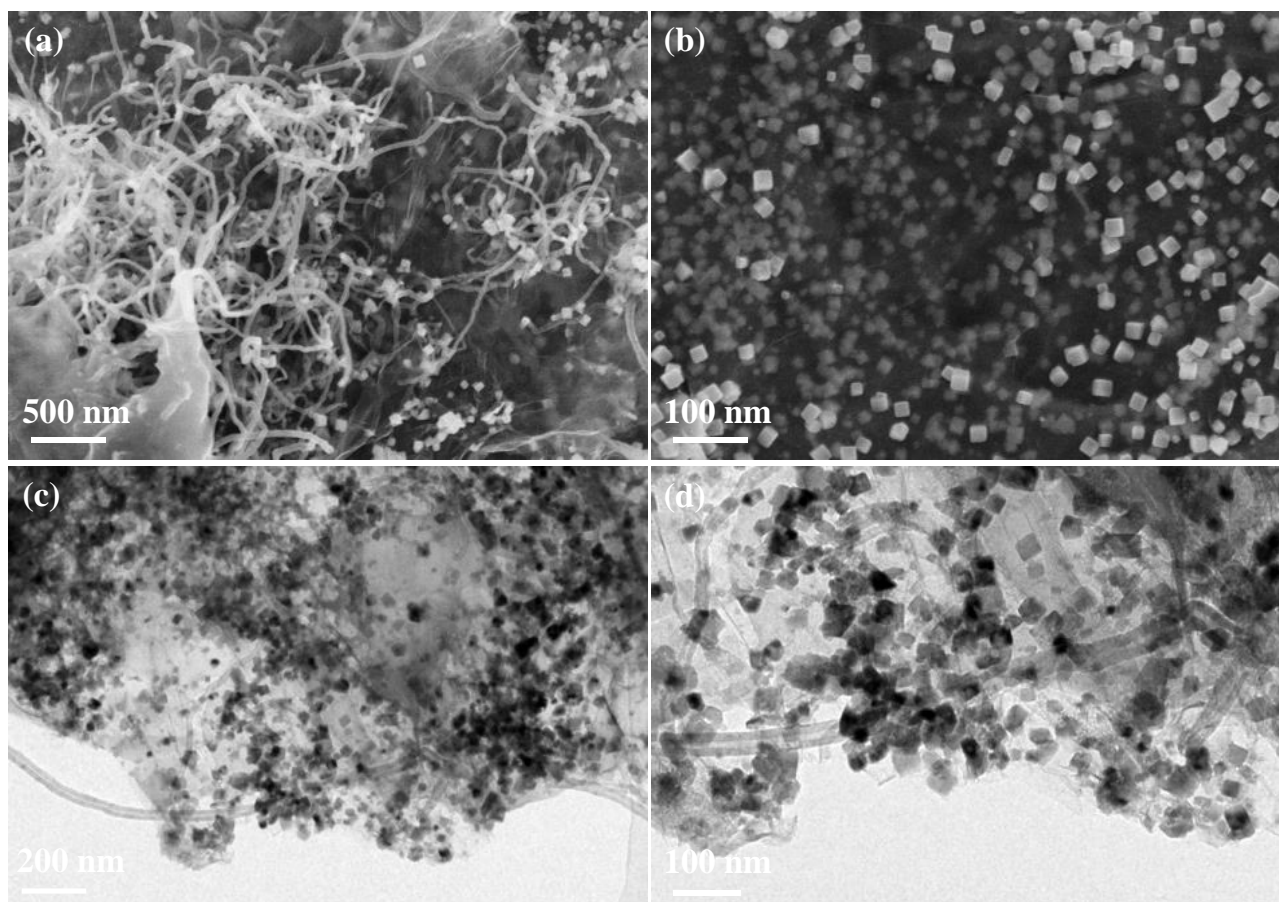


Figure 1. (a, b) SEM images and (c, d) TEM images of Pt-Cu/rGO@CNTs hybrid at different magnification.

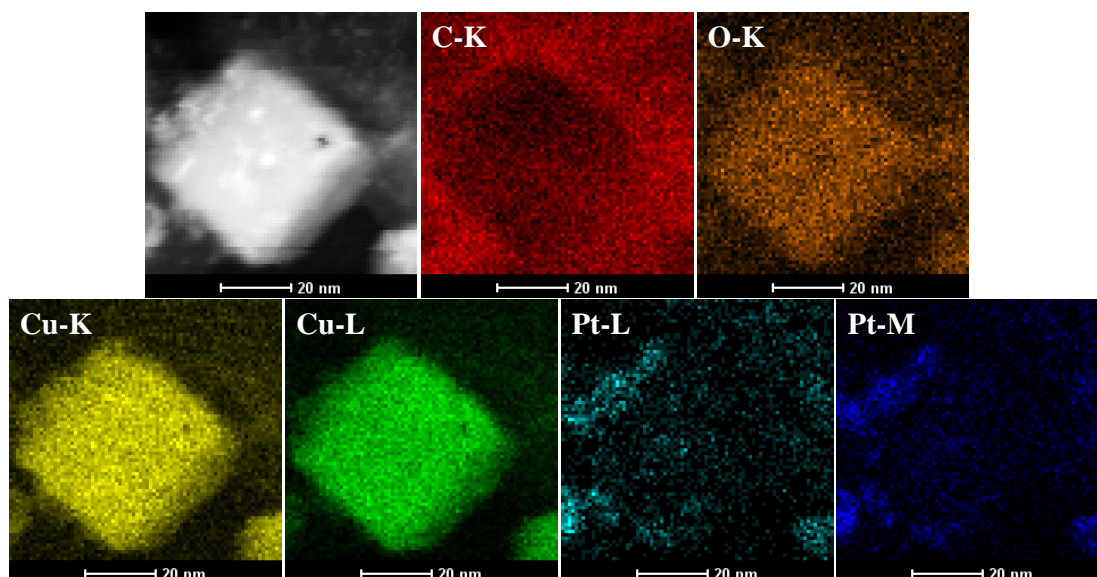


Figure 2. HAADF-STEM image and corresponding elemental mapping of Pt-Cu/rGO@CNTs hybrid.

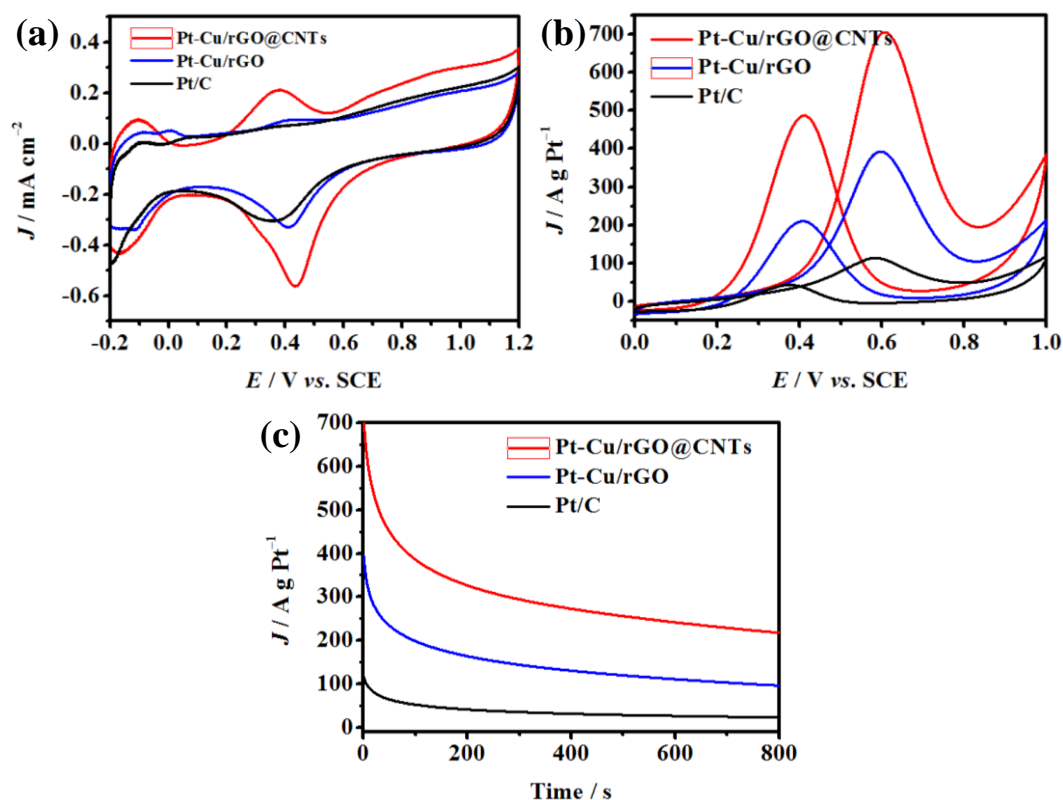


Figure 3. Cyclic voltammograms of different catalysts in N_2 -saturated $0.5 \text{ M H}_2\text{SO}_4$ (a) and $0.5 \text{ M H}_2\text{SO}_4 + 0.5 \text{ M CH}_3\text{OH}$ (b) solution; (c) Chronoamperograms at the given potential of 0.65 V for 800 s .

TEM images (Fig. 1c and d) show that the Pt-Cu nanocubes are scattered evenly on the rGO sheets and the walls of CNTs, and the size of the particles is almost identical to each other (about 20 nm , Fig. S2). HAADF-STEM mapping was employed to study the elemental distribution in the Pt-

Cu/rGO@CNTs (Fig. 2). EDX spectrum (Fig. S3) demonstrates the presence of C, O, Cu, and Pt as expected. C element is attributed to both CNTs and rGO, whereas O comes from the residual oxygen-containing groups on rGO. Moreover, the presence of Pt indicates the successful replacement of Cu with Pt. In particular, the Pt skin was uniformly distributed on the Cu surface, not on the rGO or CNTs, which is beneficial to the following electrochemical reactions [14].

Fig. 3a shows CV curves of Pt-Cu/rGO@CNTs, Pt-Cu/rGO and commercial Pt/C catalyst in N₂-saturated 0.5 M H₂SO₄ solution. The ECSA values were calculated basing on hydrogen desorption between -0.2 V and 0.05 V according to the following equation [15, 16]:

$$\text{ECSA} = \frac{Q}{m_{\text{Pt}} * 210 \mu\text{C} \cdot \text{cm}^{-2}} \quad (1)$$

Where Q represents the charge for the hydrogen desorption (μC), $210 \mu\text{C cm}^{-2}$ is the charge density required to oxidize a complete hydrogen monolayer on Pt surface, and m_{Pt} is the Pt loading (g) on the electrode. Based on the integrated area under the desorption peak in the cyclic voltammograms, the ECSA value of Pt-Cu/rGO@CNTs catalyst is calculated to be $0.07 \text{ m}^2 \text{ g}^{-1}$, which is much higher than that of commercial Pt/C ($0.03 \text{ m}^2 \text{ g}^{-1}$) and Pt-Cu/rGO ($0.04 \text{ m}^2 \text{ g}^{-1}$). Such high ECSA is ascribed to the Pt skin micro-structure (exposing more accessible Pt atom active sites) and the 3D interconnected macro-morphology induced by pristine CNTs insertion (preventing the aggregation of rGO sheets and providing more access to mass and electron transport).

The electrocatalytic activity of Pt-Cu/rGO@CNTs hybrid towards the MOR are shown in Fig. 3b. The peak current density of Pt-Cu/rGO@CNTs catalyst is found to be 704.6 A g^{-1} , which is 1.79 times and 6.17 times higher than those of Pt-Cu/rGO (392.6 A g^{-1}) and commercial Pt/C (114.2 A g^{-1}) catalyst, respectively. Additionally, the onset potential of the forward anodic peak of the Pt-Cu/rGO@CNTs (0.30 V) is obviously lower than those of Pt-Cu/rGO (0.35 V) and commercial Pt/C (0.45 V). The significant negative shift of MOR onset potential and higher peak current density suggest that the Pt-Cu/rGO@CNTs catalyst exhibits superior electrocatalytic activity. Moreover, the ratio of peak current in the forward scan (I_f) and backward scan (I_b), I_f/I_b , can be used to evaluate the tolerance of the catalysts to the intermediate carbonaceous species (especially CO) [17]. The I_f/I_b ratios of Pt-Cu/rGO@CNTs, Pt-Cu/rGO and commercial Pt/C are 1.86, 1.45 and 0.80, respectively, meaning that the Pt-Cu/rGO@CNTs catalyst possesses the strongest tolerance ability.

Table 1. Comparison of MORs for Pt-Cu/rGO@CNTs with some Pt-based electrocatalysts.

Catalysts	Peak current density (A g^{-1})	Supporting electrolyte	Methanol concentration	Ref.
PtFe/RGO	461.5	0.5 M H ₂ SO ₄	0.5 M	[18]
Pt/NGA	507.5	0.5 M H ₂ SO ₄	0.5 M	[19]
PtRu icosahedra	74.43	0.5 M H ₂ SO ₄	0.5 M	[20]
Pt/YBCPE	65.99	0.5 M H ₂ SO ₄	1.0 M	[21]
np-PtRuCuW	467.1	0.5 M H ₂ SO ₄	0.5 M	[22]
Pt-Cu/rGO@CNTs	704.6	0.5 M H ₂ SO ₄	0.5 M	This work

To objectively evaluate the electrocatalytic MOR performance of Pt-Cu/rGO@CNTs hybrid, the MOR performances for some Pt-based electrocatalysts were referred (Table 1) [18-22]. Pt-Cu/rGO@CNTs hybrid exhibited higher peak current density, indicating its better electrocatalytic activity towards methanol oxidation. These results manifested that Pt-Cu/rGO@CNTs hybrid reached the state-of-the-art level for Pt based electrocatalysts towards methanol oxidation.

Chronopotentiometry is another useful approach to study the long-term stabilities of the as-prepared catalysts (Fig. 3c). The current density of Pt-Cu/rGO@CNTs and Pt-Cu/rGO catalysts decayed slowly at the initial stage, which means a higher tolerance to carbonaceous species generated during the methanol oxidation compared to the commercial Pt/C. Compared to the Pt-Cu/rGO and Pt/C, the Pt-Cu/rGO@CNTs catalyst exhibits much higher limiting current densities during the measurement, indicating that the Pt-Cu/rGO@CNTs catalyst possesses superior durability towards methanol electrooxidation.

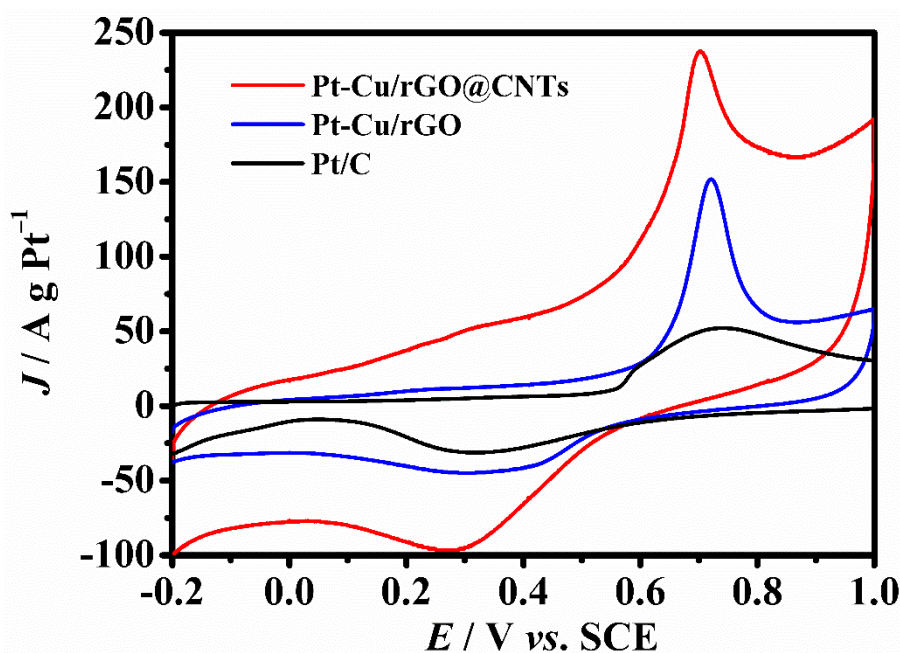


Figure 4. CO stripping cycle voltammograms of three different catalysts in N_2 -saturated 1.0 M KOH solution at a scan rate of 50 mV s^{-1} .

To explore the poison resistance of three different catalysts, electrocatalytic oxidation of pure CO molecules was investigated through the CO stripping experiments, and the cycle voltammograms are shown in Fig. 4. The onset peak potentials of CO oxidation for Pt-Cu/rGO@CNTs ($\sim 0.2 \text{ V}$) are more negative than those of Pt-Cu/rGO and commercial Pt/C ($\sim 0.6 \text{ V}$), indicating that less applied potential is required to reach the CO electrooxidation on the Pt-Cu/rGO@CNTs catalyst. The Pt-Cu/rGO@CNTs exhibit the markedly higher oxidation current density (237.4 A g^{-1}) than those of Pt-Cu/rGO (152.0 A g^{-1}) and commercial Pt/C (52.1 A g^{-1}). These results reveal that the formation of core-shell Pt-Cu micro-structure could facilitate the removal of CO out of the catalyst surface, which is in consistence with the higher electrocatalytic activity and better durability demonstrated above.

4. CONCLUSIONS

We have prepared 3D graphene-carbon nanotubes supported Cu nanocubes with Pt skin *via in situ* one-step electrodeposition and galvanic replacement method. The Pt-Cu/rGO@CNTs hybrid not only possesses binder-free 3D interconnected network allowing rapid mass diffusion and fast electron transfer, but also owns Cu nanocubes with active Pt skin with more active sites and tightly cooperation interaction to enhance anti-poison ability. Therefore, the catalyst shows excellent electrocatalytic activity and superior durability towards the MOR. Moreover, this work offers a simple and green strategy to design highly active and stable electrocatalysts that could be used in DMFCs and other energy-related applications.

ACKNOWLEDGEMENTS

This work was supported by the National Natural Science Foundation of China (Grant No. 51808279), the National Key Research and Development Program of China (Grant No. 2018YFC0406405), the Department of Education Fund of Jiangxi Province (Grant No. GJJ170616), the Open Project of Key Laboratory of Environmental Biotechnology, CAS (Grant No. kf2018009), and Doctoral Scientific Research Foundation of Nanchang Hangkong University, Jiangxi Province (Grant No. EA201702384).

SUPPORTING DATA

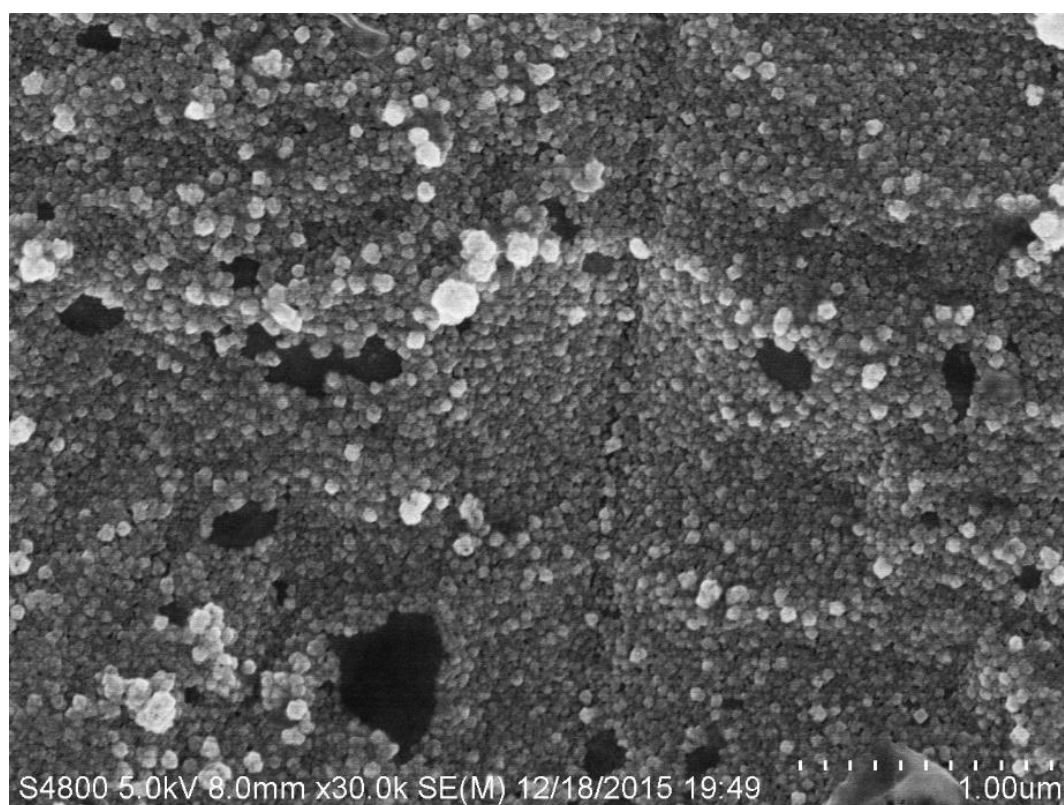


Figure S1 SEM image of flat-lying rGO nanosheets supported Cu nanoparticles.

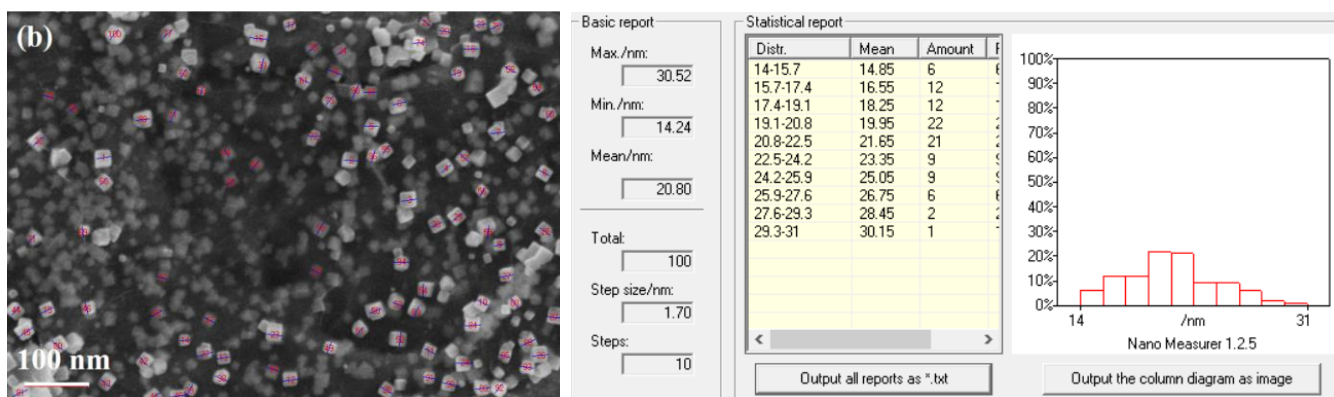


Figure S2 Histogram of statistical analysis of Pt-Cu particle size (based on 100 randomly picked particles).

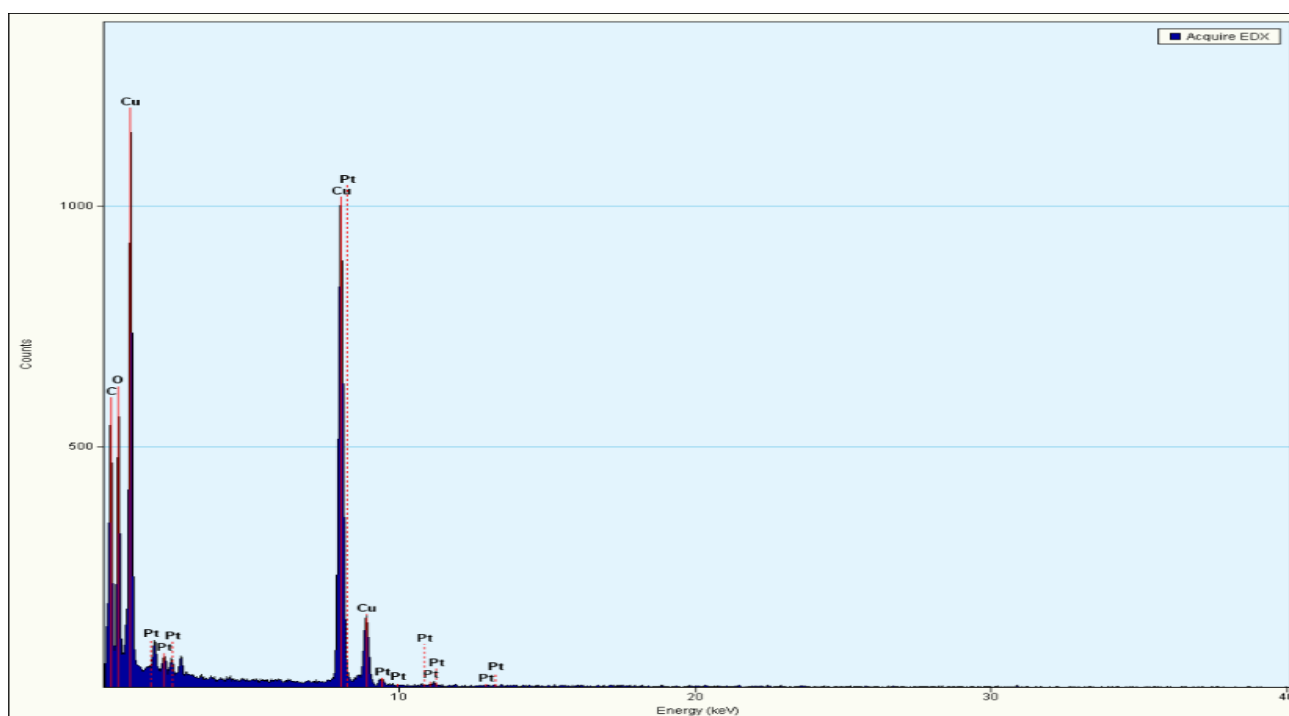


Figure S3 EDX spectrum of Pt-Cu/rGO@CNT hybrid.

References

1. L. Z. Zou, P. H. Shao, K. Zhang, L. M. Yang, D. You, H. Shi, S. G. Pavlostathis, W. Q. Lai, D. H. Liang and X. B. Luo, *Chem. Eng. J.*, 364 (2019) 160.
2. P. H. Shao, J. Y. Tian, X. G. Duan, Y. Yang, W. X. Shi, X. B. Luo, F. Y. Cui, S. L. Luo and S. B. Wang, *Chem. Eng. J.*, 359 (2019) 79.
3. P. Shao, J. Tian, F. Yang, X. Duan, S. Gao, W. Shi, X. Luo, F. Cui, S. Luo, and S. Wang, *Adv. Funct. Mater.*, 28 (2018) 1705295.
4. W. Huang, H. Wang, J. Zhou, J. Wang, P. N. Duchesne, D. Muir, P. Zhang, N. Han, F. P. Zhao, M. Zeng, J. Zhong, C. H. Jin, Y. G. Li, S. T. Lee and H. J. Dai, *Nat. Commun.*, 6 (2015) 10035.

5. C. Chen, Y. Kang, Z. Huo, Z. Zhu, W. Huang, H. L. Xin, J. D. Snyder, D. G. Li, J. A. Herron, M. Mavrikakis, M. F. Chi, K. L. More, Y. D. Li, N. M. Markovic, G. A. Somorjai, P. D. Yang and V. R. Stamenkovic, *Science*, 343 (2014) 1339.
6. X. Xu, X. Zhang, H. Sun, Y. Yang, X. Dai, J. Gao, X. Li, P. Zhang, H. H. Wang, N. F. Yu and S. G. Sun, *Angew. Chem.*, 126 (2014) 12730.
7. S. Bai, C. Wang, M. Deng, M. Gong, Y. Bai, J. Jiang and Y. Xiong, *Angew. Chem. Int. Ed.*, 53 (2014) 12120.
8. B. Y. Xia, H. B. Wu, Y. Yan, H. B. Wang and X. Wang, *Small*, 10 (2014) 2336.
9. X. Chen, Z. Cai, X. Chen and M. Oyama, *Carbon*, 66 (2014) 387.
10. Y. Cheng, S. Lu, H. Zhang, C. V. Varanasi and J. Liu, *Nano Lett.*, 12 (2012) 4206.
11. T. Sun, Z. Zhang, J. Xiao, C. Chen, F. Xiao, S. Wang and Y. Liu, *Sci. Rep.*, 3 (2013) 2527.
12. H. Li, K. Shin and G. Henkelman, *J. Chem. Phys.*, 149 (2018) 174705.
13. A. Mondal and N. R. Jana, *ACS Catal.*, 4 (2014) 593.
14. L. M. Yang, Z. L. Chen, D. Cui, X. B. Luo, B. Liang, L. X. Yang, T. Liu, A. J. Wang, and S. L. Luo, *Chem. Eng. J.*, 359 (2019) 894.
15. Y. Li, W. Gao, L. Ci, C. Wang and P. M. Ajayan, *Carbon*, 48 (2010) 1124.
16. S. M. Choi, M. H. Seo, H. J. Kim and W. B. Kim, *Carbon*, 49 (2011) 904.
17. L. Zhang, L. X. Ding, H. Chen, D. Li, S. Wang and H. Wang, *Small*, 13 (2017) 1604000.
18. X. Qiu, T. Li, S. Deng, K. Cen, L. Xu and Y. Tang, *Chem. Eur. J.* 24 (2018) 1246.
19. L. Zhao, X. L. Sui, J. Z. Li, J. J. Zhang, L. M. Zhang, G. S. Huang and Z. B. Wang, *Appl. Catal. B- Environ.* 231 (2018) 224.
20. Z. Lin, W. Chen, Y. Jiang, T. Bian, H. Zhang, J. Wu, Y. Wang and D. Yang, *Nanoscale* 8 (2016) 12812.
21. Y. Zhang, F. Li, X. Liu, J. Lu and G. Zhang, *Electrochim. Acta.* 242 (2017) 165.
22. X. Chen, H. Wang, Y. Wang, Q. Bai, Y. Gao and Z. Zhang, *Catalysts* 5 (2015) 1003.